FUZZY LOGIC CONTROLLER FED COORDINATED CONTROL STRATEGY FOR HYBRID *POWER* SYSTEM BASED ON VARIABLE SPEED DIESEL GENERATOR

R.Lakshmanna, PG Student, Department of Electrical and Electronics Engineering, JNTUA College of Engineering, Anantapur, India

Smt.N.Swathi, Assistant Professor(Adhoc), Department of Electrical and Electronics Engineering, JNTUA College of Engineering, Anantapur, India

Prof.R.Kiranmayi, Professor, Department of Electrical and Electronics Engineering, JNTUA College of Engineering, Anantapur, India

ABSTRACT

The installation of a control system for a hybrid off-grid system that combines a solar photovoltaic array with a diesel generator with variable speed. By employing vector-based and stator flux-oriented frame-based techniques to manage back-to-back linked converters, stability in AC voltages and system frequency regulation are guaranteed. To optimize fuel consumption, a customized control strategy is designed to modify the speed of the diesel engine. The DC-link voltage and battery current are controlled using a double-loop control method to mitigate the sluggish dynamics of variable speed operation and preserve power balance. In addition, the perturbation and observation approach is linked with the dynamic model of the DC-DC boost converter to provide effective maximum power point tracking (MPPT). to stop overshooting when the fuzzy controller makes abrupt shifts. To show the efficacy of coordinated control under varying loads and weather circumstances, the performance is achieved using MATLAB/Simulink and confirmed in the real-time hardware.

Keywords:-doubly-fed induction generator (DFIG), battery energy storage, coordinated control, maximum power point tracking, fuzzy controller, fuel-efficient hybrid off-grid system.

I.INTRODUCTION

In remote and remote places around the globe, diesel generators (DG) are now the most favored alternative for generating energy due to their dependability. This application adds a 30-kW photovoltaic (PV) array to a 14.92-kw diesel generator (DG) that runs on a fixed-speed machine. This reduces the DG's noise and pollution while also increasing fuel economy and DE efficiency under light load. From an economic perspective, this technique works well, but it exacerbates the low generator loading issue, which leads to inefficient combustion and reduced diesel engine efficiency (DE).

This problem is examined in the context of diesel engine applications that use variable speed machine technology. With light loads, the variable speed operation performs satisfactorily in terms of fuel economy and DE efficiency. This system's sluggish dynamic response, particularly during transitions and at rapid load and wind speed fluctuations, is its principal flaw.

Consequently, the control of a hybrid off-grid configuration based on a diesel generator with variable speed and solar photovoltaic array is necessary to address the problems linked to continuous power supply. Stator flux-oriented frame-based control and vector-based control are used to manage back-to-back linked converters in order to guarantee a stable functioning with the ac voltages and system frequency management. to modify the diesel engine's speed in accordance with a certain fuel consumption. A successful control plan is created. In addition, the perturbation and observation approach is linked with the de-de boost converter's dynamic model to achieve smooth and effective maximum power point tracking (MPPT). A back-calculation anti-windup scheme is incorporated into all proportional-integral controllers to prevent overshoots during the abrupt transition.

However, using an AWPl Controller will result in a system with a low-speed response and severe harmonic distortions. Fuzzy Logic Controller is used in place of AWPI Controller to solve these problems. This improves the system's fast reaction and eliminates errors.Matlab/Sim link software may be used to examine the simulation results.

II. CONFIGURATION AND OPERATION

Figure 1 depicts that, A hybrid off-grid setup is made available. It is made up of a DE-driven variable speed DFIG, with a circuit breaker (CB) connecting the stator terminals and back-to-back converters connecting the rotor terminals of the DFIG to the PCC. When DE is switched off, the CB is utilized to detach the DFIG stator from PCC and reconnect it when the weather is suitable. DC-DC boost and DC-DC buck-boost converters link the battery energy storage (BES) and the SPA to the common DC bus, respectively. The dc side is coupled to a dc dump load, which prevents overcharging of BES. This OFF-grid configuration allows for fuel economy at light loads as well as when the DE is turned off. The DG runs at variable speed based on the current load power demand (P_L), maximum and minimum rated load power demand (P_n), generated power from the SPA (P_{SPA}), and state of charge of the BES (SoC%).

III. CONTROLLER FOR OFF-GRID SYSTEM

The established coordinated control approach, as well as the control techniques for the dc-dc buck-boost converter, DC-DC boost converter, and RSC LSC, are provided in this part.

A. Coordinated Control Strategy

The VSDG model and its coordinated control approach are displayed in Fig. 2. The speed regulator, actuator, engine, and DFIG make up the model. Further information on the parameter design and the actuator and engine mathematical models is provided in. The governor provides the precise fuel economy, while the actuator regulates the DE speed. The ideal DE speed curve, coordinated control algorithm, and speed controller make up the block in charge of DE speed control. In, the specifics of DFIG control are covered. As shown in Table I, the coordinated control method uses nine modes to provide the reference power (P_{DFIG}^*). Depending on the operating conditions, the DFIG operates in both supersynchronous and subsynchronous generating modes.

B. Control of RSC

An enhanced vector control based on AWPI controllers is displayed in Fig. 3. High performance in a range of DE speed situations and providing the necessary magnetizing current to the DFIG are the two purposes of RSC control. As seen in Fig. 1, the DFIG stator receives its excitation from BES via LSC. To derive the quadrature axis component of RSC current, the proportional-integral controller (AWPI) with antiwindup feedback is fed the

reference rotor speed (w_r^*) compared to the measured value (w_r) and the rotor speed error (Δw_r).
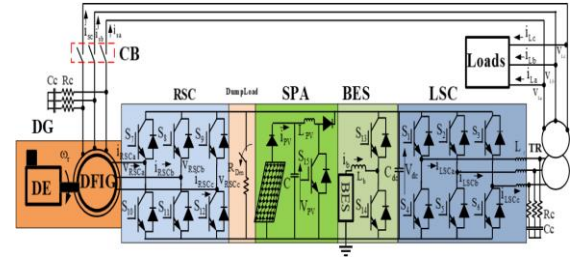
Fig. 1. Studying a hybrid off-grid system with variable speed DG and SPA.
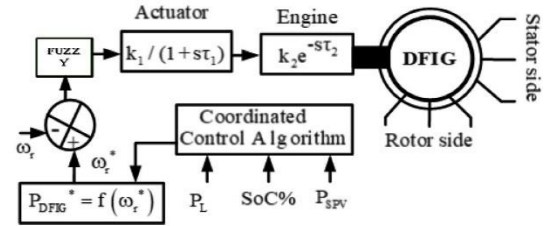
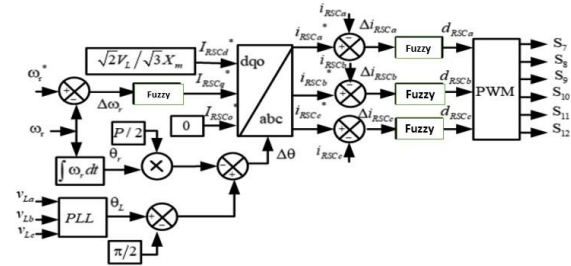

Fig. 2. The coordinated control approach of the DE model.

Fig. 3. Vector-oriented management for RSC

TABLE I

Operational Techniques of the Hybrid Off-Grid System

MODES	Conditions	State of VSDG	State of BES
1	SoC%=80%, $P_L \geq 0.8P_n$, $P_{SPA} \geq P_L$	Turned off	Stop charging
2	SoC%>80%, $P_L \geq 0.8P_n$, $P_{SPA} \geq P_L$	Turned off	Stop charging Activate dump load
3	50%≤SoC%≤80%, $P_L \geq 0.8Pn$, $P_{SPA} < P_L$	Turned off	BES Discharging

4	50%≤SoC%≤80%, $P_L 0.8≥Pn$, $P_{SPA}≥P_L$	Turned off	BES charging
5	SoC%≤50%,0.3Pn $<P_L < 0.8P_n$, $P_{SPA}=P_L$	Sub-synchronous	charging BES
6	SoC%≤50%, 0.3Pn$<P_L <$ 0.8P_n, PSPA=0	Super-synchronous	Fast charging BES
7	SoC%≤50%, 0.3Pn$<P_L<$0.8P_n, $P_{SPA}<P_L$	Super-synchronous	Fast charging BES
8	50%≤SoC%<80%, 0.3Pn$<P_L$, $P_{SPA}≥0$	Sub-synchronous	Charging BES
9	SoC% ≥80%, 0.3Pn$<P_L<$0.8Pn, PSPA ≤PL	Turned off	Stop charging BES

$$\left(I^*_{RSCq}\right)As$$

$$I^*_{RSCq} = k_{p1} + \Delta w_r + \left(k_{i1} - \frac{e_1}{T_{a1}}\right)\int_0^t \Delta w_r \, dt$$

where the terms PI controller gains, error between the saturated and unsaturated control signal, and antiwindup gain—which is chosen to be equal to proportional gain—are represented by the variables kp1, ki1, e_1e_1, and T_{a1}. Assuming the rated magnetizing current (I_{msr}), the direct axis component of RSC current (I^*_{RSCd}) is computed as

$$I^*_{RSCd} = I_{msr} = \frac{\sqrt{2}V_L}{\sqrt{3}X_m}$$

where V_L is the line voltage at the stator terminals and X_m is the DFIG's magnetizing reactance. The RSC current references $(i^*_{RSCa} i^*_{RSCb} \, and \, i^*_{RSCc})$ are acquired by the application of the inverse Park's Transformation.

$$[I^*_{RSC(abc)}] = T_{dqo}(\Delta\theta)^{-1}[I_{RSC(abc)^*}]$$

where the inverse Park's transformation is represented by $T_{dqo}(\Delta\theta)^{-1}$ and may be written as

$$\begin{bmatrix} \cos(\Delta\theta) & \sin(\Delta\theta) & 1 \\ \cos(\Delta\theta - \frac{2\pi}{3}) & \sin(\Delta\theta - \frac{2\pi}{3}) & 1 \\ \cos(\Delta\theta + \frac{2\pi}{3}) & \sin(\Delta\theta - \frac{2\pi}{3}) & 1 \end{bmatrix}$$
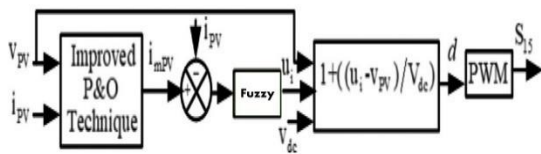
Fig. 4. Speed converter DC–DC control scheme. When the rotor transformation angle, denoted by Δθ, is determined as

$$\Delta\theta = \left(\theta_s - \frac{\pi}{2}\right) - \left(\frac{P}{2}\right)\theta_r$$

where P stands for the number of DFIG poles, and θr, θs, and rotor angles, respectively. The phased locked loop is utilized to produces, while the rotor speed is integrated to obtain θr.

$$\Delta\theta = \int_0^t w_r dt$$

The duty cycles $(d_{RSVa}, d_{RSCb} \, and \, d_{RSCc})$ are obtained by comparing the estimated reference rotor currents with measured RSC currents.

$$d_{RSCa} = k_{p2}\Delta i_{RSCa} + \left(k_{i2} - \frac{e_2}{T_{a2}}\right)\int_0^t \Delta i_{RSCa} \, dt$$

$$d_{RSCb} = k_{p2}\Delta i_{RSCb} + \left(k_{i2} - \frac{e_2}{T_{a2}}\right)\int_0^t \Delta i_{RSCb} \, dt$$

$$d_{RSCc} = k_{p2}\Delta i_{RSCc} + \left(k_{i2} - \frac{e_2}{T_{a2}}\right)\int_0^t \Delta i_{RSCc} \, dt$$

where the values of the AWPI controller gains of the inner loop, the error between the saturated and unsaturated control signals, the antiwindup gain, and kp2, ki2, e2, and T_{a2} are indicated, respectively. A PWM controller receives the obtained duty cycles and uses them to generate a switching signal for $(S_7 - S_{12})$.

C. Control of DC–DC Boost Converter

The designed dc-dc boost converter control method is shown in Figure 4. The dynamic model of the dc-dc boost converter and the enhanced P&O approach described in are used to produce excellent performance from SPA during changes in solar irradiation. The P&O approach is used to determine the reference PV current (i_{mPV}). The difference between the measured SPA current (I_{PV}) and I_{mPV} is sent to the PI current controller with antiwindup feedback as

$$u_i = k_{p3}\left(I_{mPV} - k_{PV}\right) + \left(k_{i3} - \frac{e_3}{T_{a3}}\right)\int_0^t (I_{mPV} - P_{PV}) \, dt$$

The variables kp3, ki3, e3, and Ta3 represent the proportional and integral gains of the controller, the antiwindup gain, and the error between the saturated and unsaturated control signals, respectively. The dynamic model of the dc-dc boost converter and the output of the PI controller (u_i) are used to determine the duty cycle (d).

$$d = 1 + \frac{u_i - V_{PV}}{V_{dc}}$$

To acquire the switching signal for the switch , feed the obtained duty cycle (d) to the PWM controller.
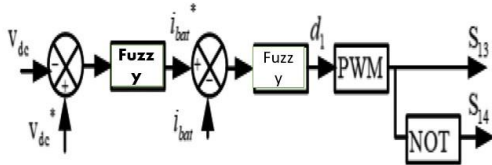
Fig. 5. Control system for buck-boost dc-dc converter.
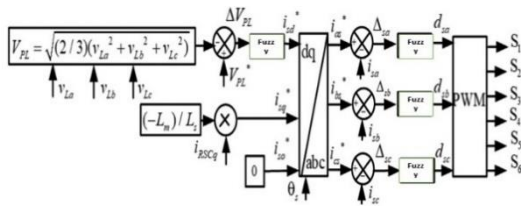
Fig. 6. Control algorithm for LSC

D. Control of DC–DC Buck–Boost Converter

The designed control algorithm for the DC-DC buck-boost converter is shown in Fig. 5. Double-loop control is created to balance power in an off-grid system, correct for SPA intermittency, and provide uninterrupted power to linked loads, particularly during VSDG speed changes and the transition between DFIG operating modes. The reference BES current (i^*_{bat}) may be found by using

$$i^*_{bat} = k_{p4}(V^*_{dc} - V_{dc}) + \left(k_{i4} - \frac{e_4}{T_{a4}}\right)\int_0^t (V^*_{dc} - V_{dc})dt$$

where the variables k_{p4}, k_{i4}, e_4 and T_{a4}, Vdc, and V^*_{dc} stand for the antiwindup gain, dc-link voltage, and its reference, the proportional and integral gains of the outer control loop, and the error between the saturated and unsaturated control signal, respectively. To get the duty cycle (d_1) and produce the switching signal for S_{13} and S_{14}, the measured BES current (i_{bat}) is compared to its reference ibat∗. The BES current error is then provided to the PI controller with antiwindup feedback.

E. Control of LSC

Figure 6 presents the load side converter (LSC) control method. Stator fluxoriented frame-based control is used to provide power to PCC and to keep the system frequency and ac voltage constant. The stator current's reference d-component (i^*_{sd}) is calculated as

$$i^*_{sd} = k_{p5}\Delta V_{PL} + \left(k_{i5} - \frac{e_5}{T_{a5}}\right)\int_0^t \Delta V_{PL} dt$$

The reference amplitude of PCC voltage (V^*_{PL}) given in and its measured value (V_{PL}), as well as the error between the saturated and unsaturated control signals, anti-windup gain, and ΔV_{PL} denote

proportional and integral gains of the controller, as well as the error in PCC voltage.

$$V_{PL} = \sqrt{\left(\frac{2}{3}\right)(v_{La}^2 + v_{Lb}^2 + v_{La}^2)}$$

where the observed PCC voltages are denoted by V_{La}, V_{Lb} and V_{Lc}

The stator current in the q-axis (i^*_{sq}), is derived as

$$i^*_{sq} = -(L_m/L_S)i_{RSCq}$$

where the RSC current in the q-axis and the mutual, stator, and i^*_{RSCq} inductances are shown. In order to achieve system frequency management, LSC is made to run at 60 Hz as

$$\theta_s = 2\pi f_s t$$

When sampling time (t) and the stator frequency (fs), which is 60 Hz, are shown respectively. The inverse Park Transformation matrix is used to derive the stator's reference currents (i^*_{sa}, i^*_{sb} and i^*_{sc}) as

$$[i^*_{sabc}] = T_{dqo}(\theta_S)^{-1}[I^*_{sdqo}]$$

$$d_{sa} = k_{p6}\Delta i_{sa} + \left(k_{i6} - \frac{e_6}{T_{a6}}\right)\int_0^t \Delta i_{sa}\, dt$$

$$d_{sb} = k_{p6}\Delta i_{sb} + \left(k_{i6} - \frac{e_6}{T_{a6}}\right)\int_0^t \Delta i_{sb}\, dt$$

$$d_{sc} = k_{p6}\Delta i_{sc} + \left(k_{i6} - \frac{e_6}{T_{a6}}\right)\int_0^t \Delta i_{sc}\, dt$$

where PI, controller gains of inner control loops, error between the saturated and unsaturated control signal, and antiwindup gain are represented by the variables k_{p6}, k_{i6}, e_6 and T_{a6} respectively. The PWM controller receives the obtained duty cycles and uses them to generate the switching signal for ($S_1 - S_6$).

IV.Proposed Method Of Fuzzy Logic Controller:-

By enabling the meaningful use of incomplete knowledge, fuzzy logic reduces complexity. It can be put into practice via software, hardware, or a mix of the two. Stated differently, the fuzzy logic method to problem solving simulates human decision-making processes, but at a far quicker pace. Fuzzy logic requires descriptions or numbers to be expressed in order to function. For instance, the speed can be described as "slow" or as the value 5 m/s. When used by various people, the term "slow" might have varied meanings, thus it's important to interpret it in light of the surrounding circumstances. Certain values are simple to categorize, while others may be more challenging due to the limitations of human comprehension in certain contexts.

When discussing the same pace, one person may think it's "slow," while another may argue it's "not fast." So-called fuzzy sets can be used to assist discern between these discrepancies. The four main components shown in Figure 2 are often used to develop a fuzzy logic control system: the defuzzification interface, fuzzy inference engine, fuzzy rule matrix, and fuzzification interface.
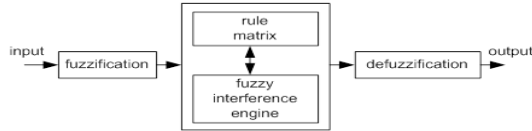
Figure .7. Fuzzy logic controller

Member ship function:-
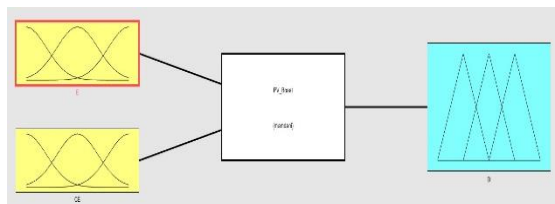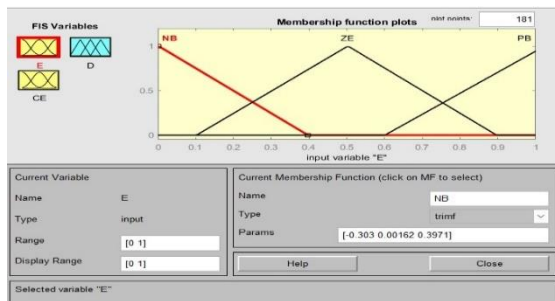
Rules:-
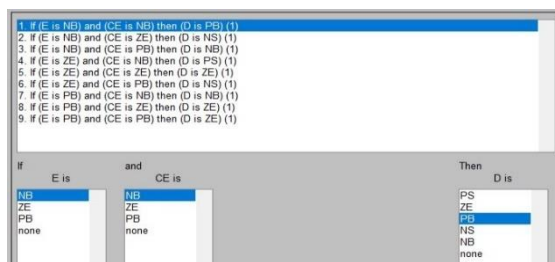
V.MODES OF OPERATION :-
Modes 1 and 2:-

This system turns on by turning off the VSDG in Mode 1, opening the CB, and halting the battery charge. It initiates the dump load in Mode 2. Both modes are designed to safeguard the BES, save fuel, and operate steadily. As indicated in Table I, this OFF-grid system functions in Mode 1 only in the following scenarios: SoC% = 80%, $P_L \geq 0.8Pn$, and

$P_{SPA} \geq P_L$; in Mode 2, it functions only in the following scenarios: SoC% > 80%, $P_L \geq 0.8$ Pn, and $P_{SPA} \geq P_L$. Figure 8(a) illustrates this with zero rotor speed and VSDG current (stator and rotor currents) when the load current is matched by the LSC current. When switching between AC voltage and frequency, one notices that they are both well controlled and do not overshoot.

Modes 3 And 4:-

Although the VSDG is still off, the system in question begins battery drain in Mode 3 and charges it in Mode 4. Both modes are designed for steady and fuel-efficient operation. The OFF-grid system functions in Mode 4 only if the 50%≤SoC%≤80%, $P_L > 0.8Pn$, and $P_{SPA} \leq P_L$, as shown in Table I. In Fig. 9(a), the output LSC current equals the load current, and the stator and rotor currents, together with the DFIG rotor speed, are all equal to zero. This indicates that the load is exclusively provided by the LSC and that the VSDG is switched off.

Modes 5,6 and 7:-

In order to confirm the fuel-saving operation and sluggish dynamics adjustment under variable speed, the system's performance is simulated. The OFF-grid system runs in Modes 8 and 9 only if the following requirements are met: 50%≤SoC%< P_L. These are the conditions shown in Table I.
Modes 8 and 9:-

To confirm the system's stability and fuel efficiency under abrupt load increases and decreases, its performance is simulated. The OFF-grid system functions in Modes 8 and 9 according to the requirements listed in Table I, but only if 50%≤SoC%< P_L.

Parameter specifications Of DFIG:-

14.92KW of stator power, 460V of line-to-line voltage, 60 Hz frequency, 1500 rpm of actual speed, 1761.84 rpm of maximum speed, and 184.3 radians per second of rotor speed are all listed.
SPA Parameters:-
   Maximum rated power =220.5 W ,O.C Voltage =36.3V , S.C Current =7.84 A , V_{mp}=30 V I_{mp}=7.35 A , Temperature =25C , Irradiation =1000 W\M2.
Battery parameters:-
   Nominal voltage =12 v , Rated capacity =12 A , Initial-State-of-charge =50%

VI.SIMULATION RESULTS

AWPI Controller Result :-
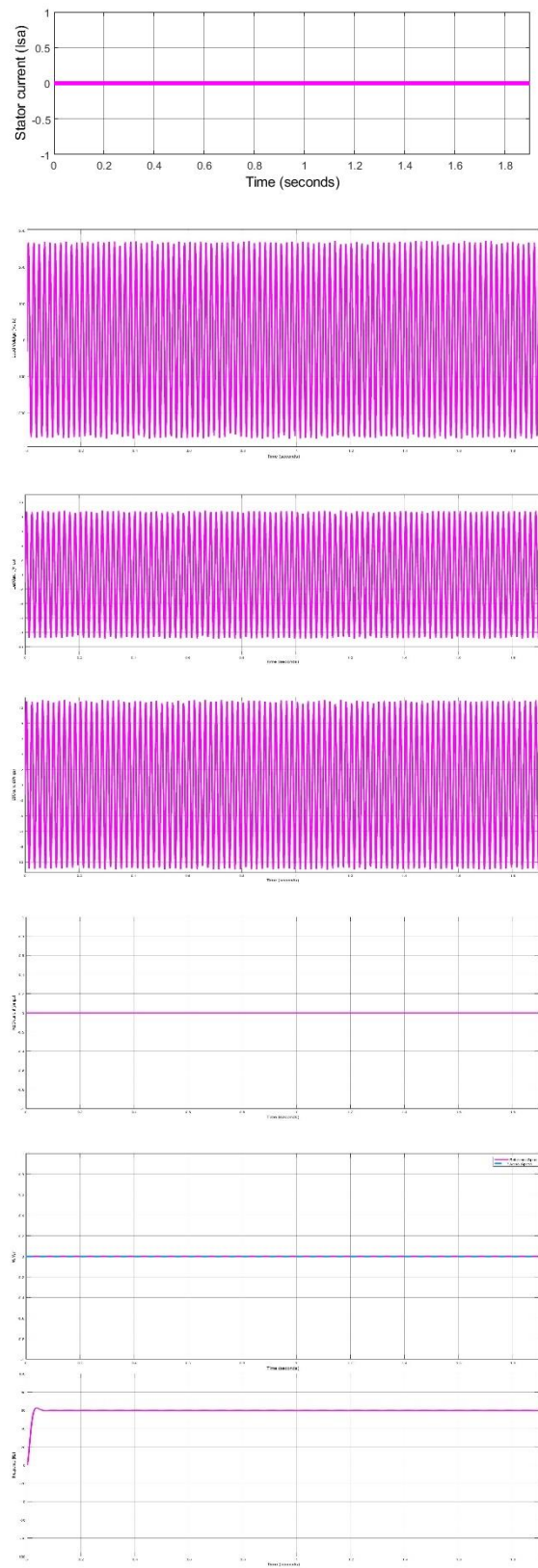
FUZZY Controller Results :-

(a)
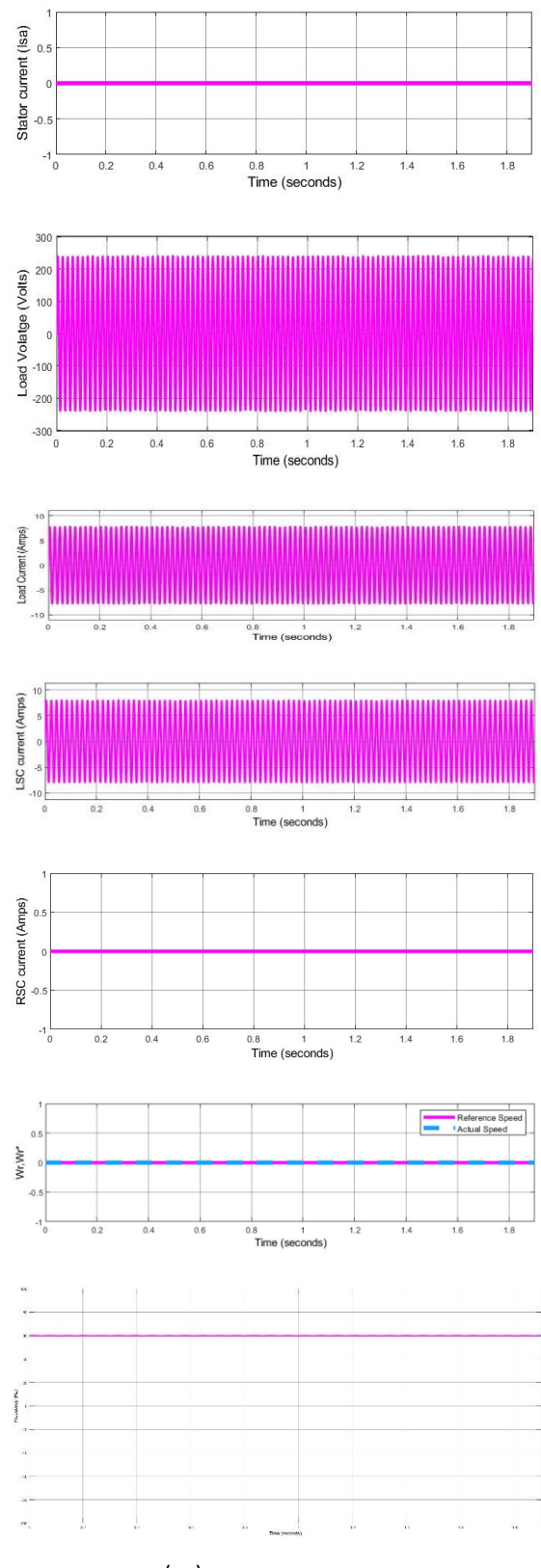
(a)
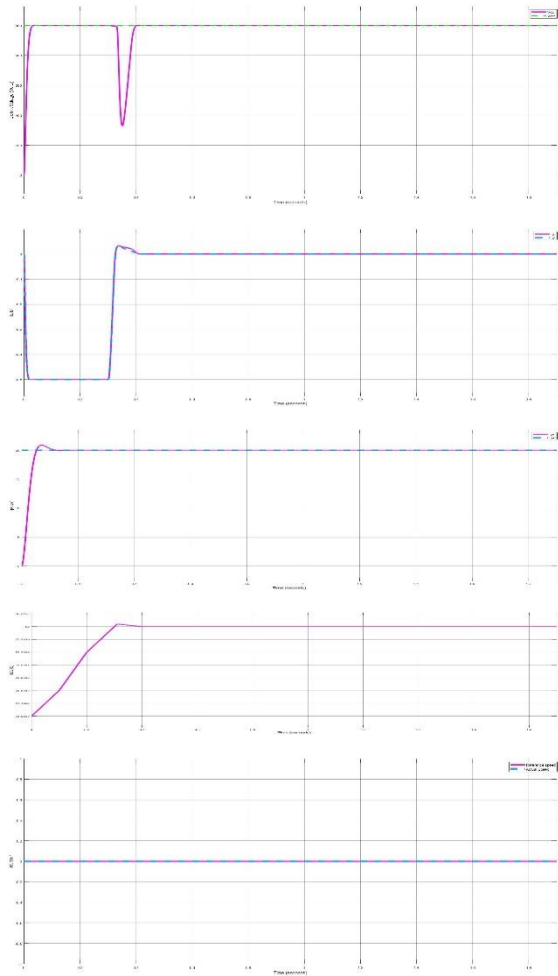
(b)
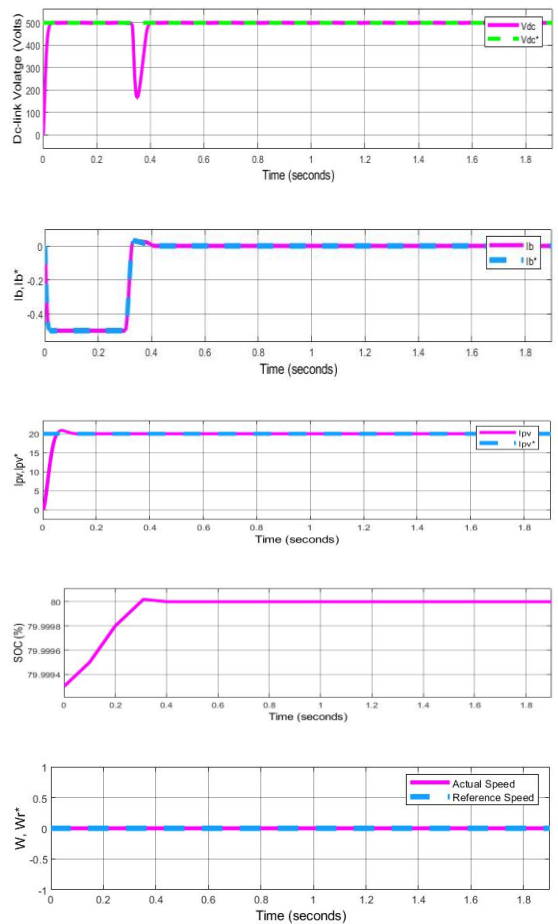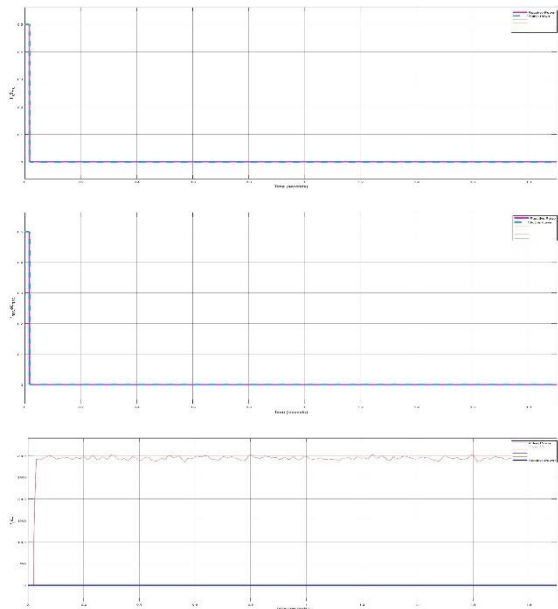
(b)
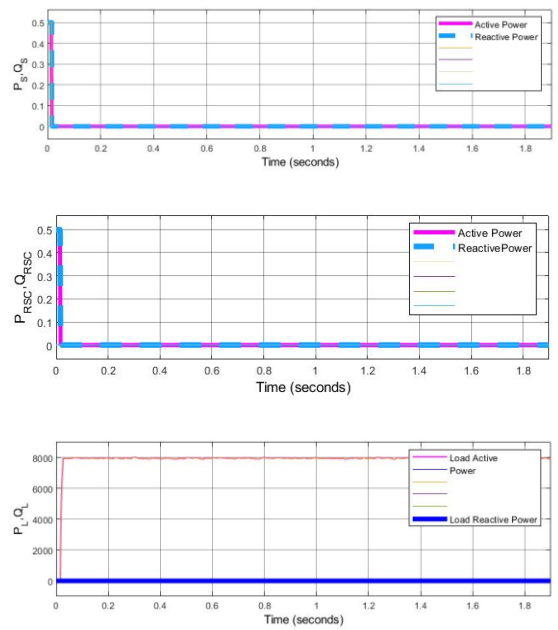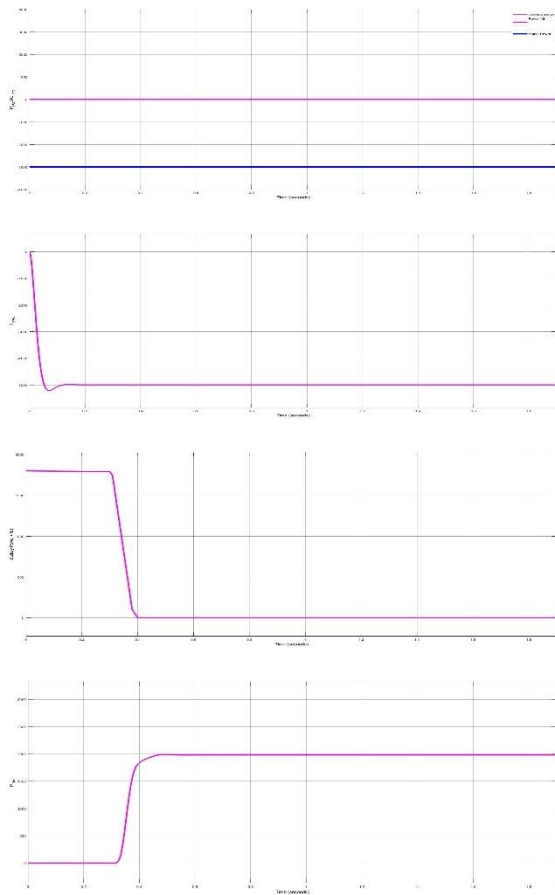
(c)

Fig. 8. Dynamic performance while the system is in Modes 1 and 2, at the ac side, dc side, and power flow.
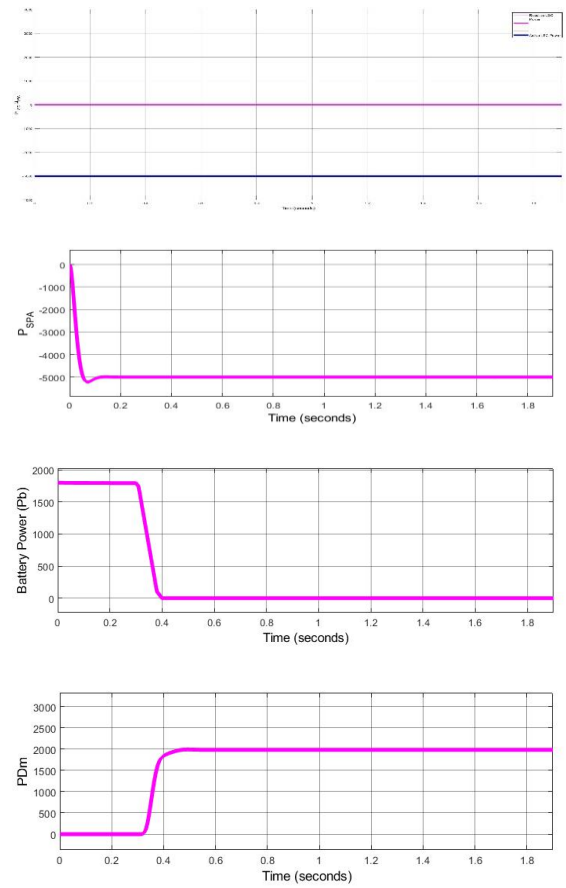
(c)

Fig. 8. Dynamic operation of the system in Modes 1 and 2, at the ac side, dc side, and power flow.
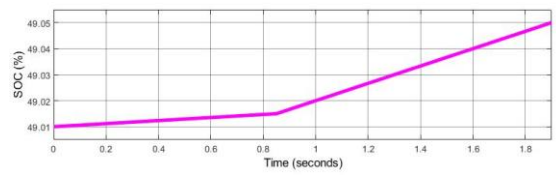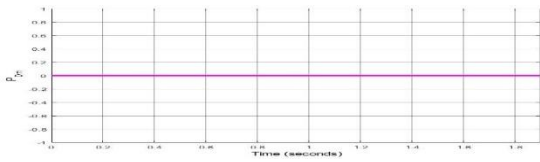
(a)

(b)

(a)
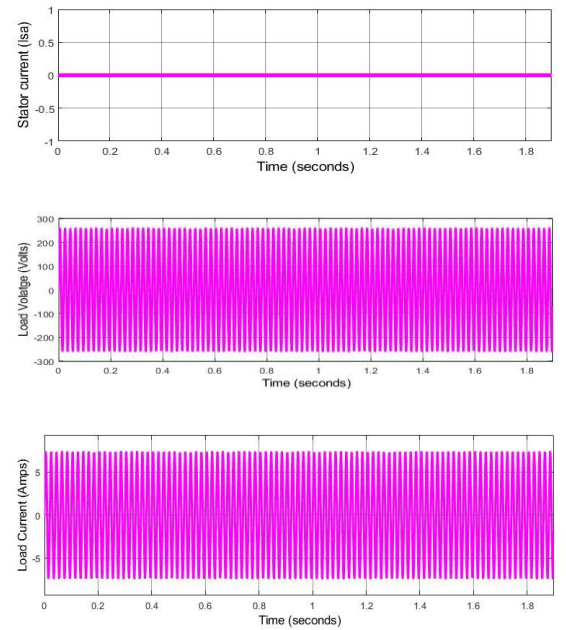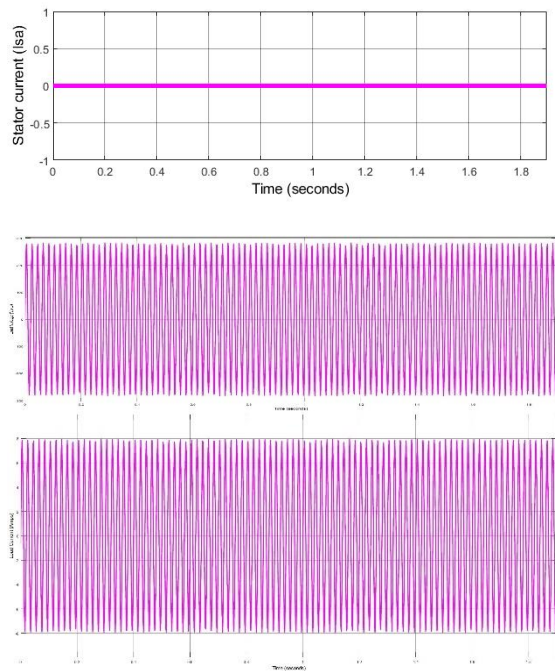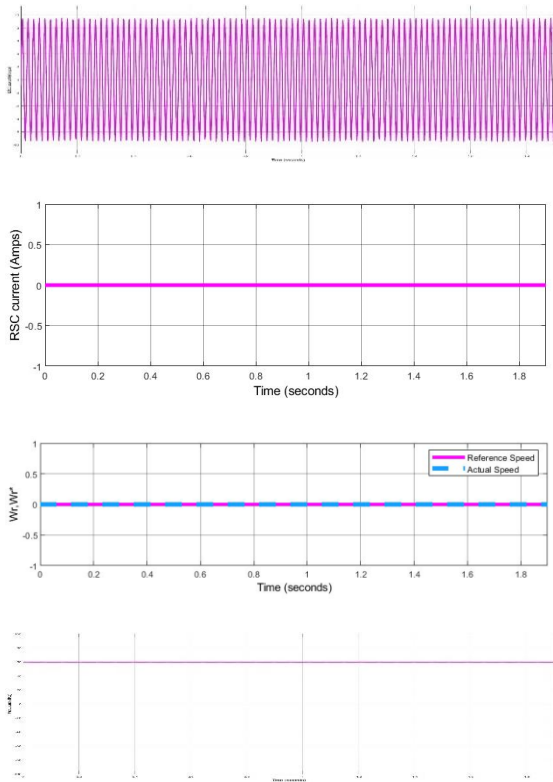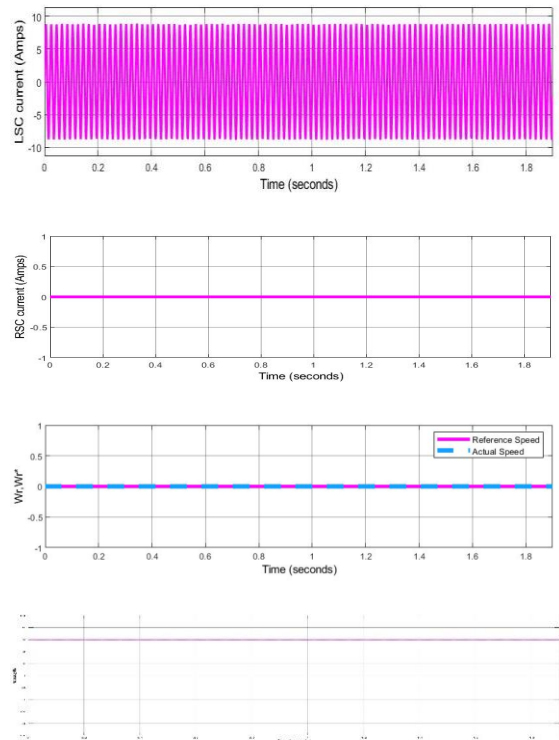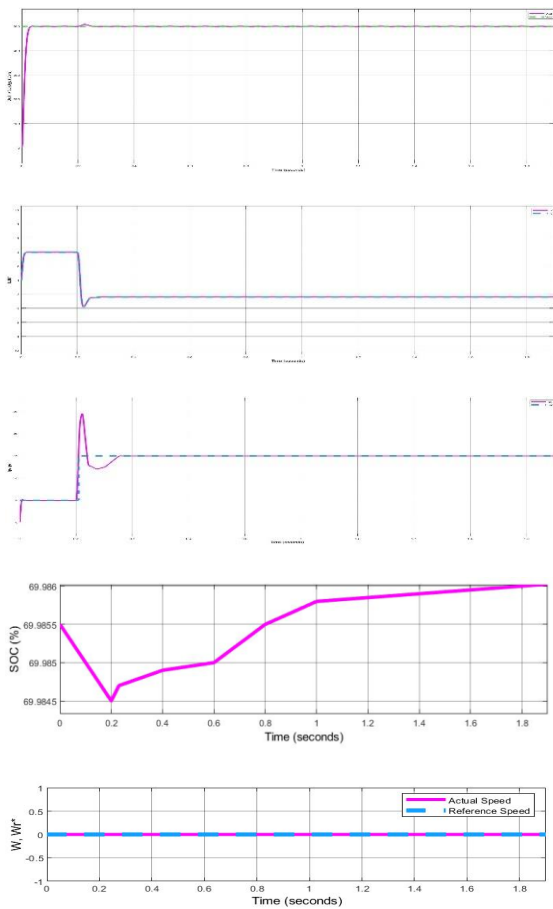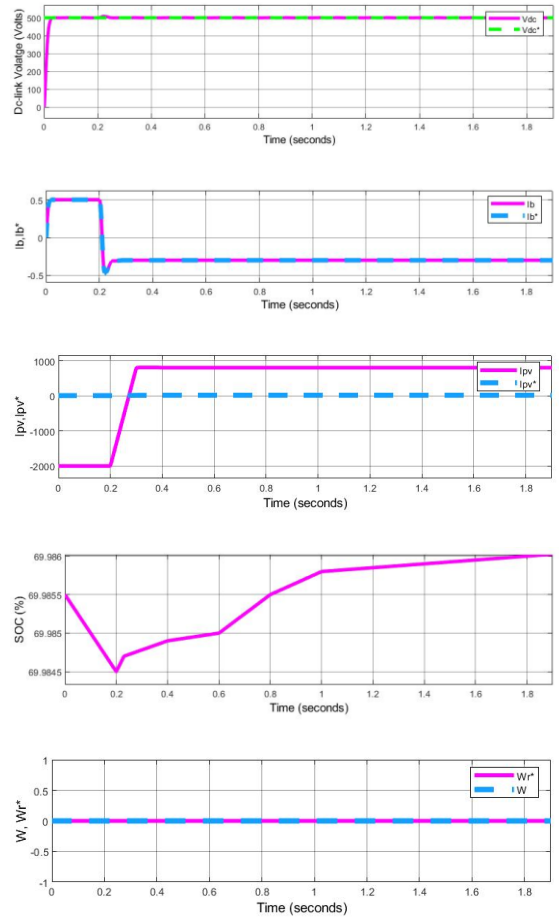
(b)
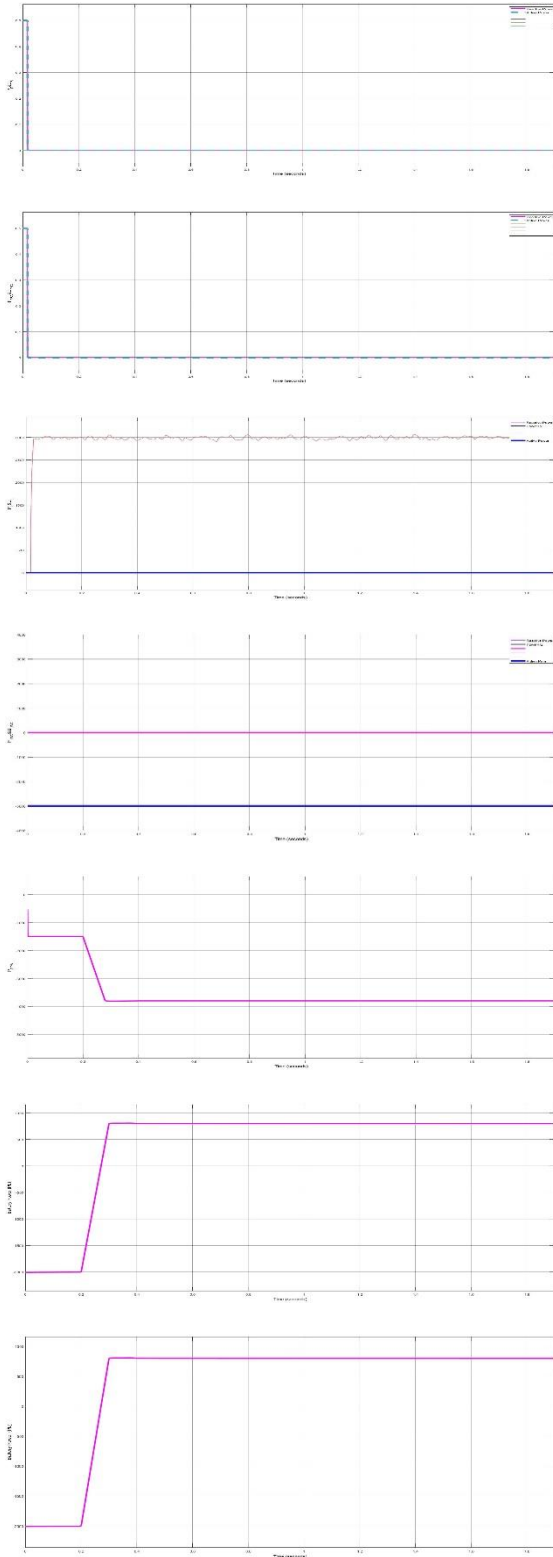
(c)

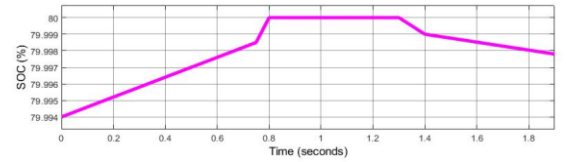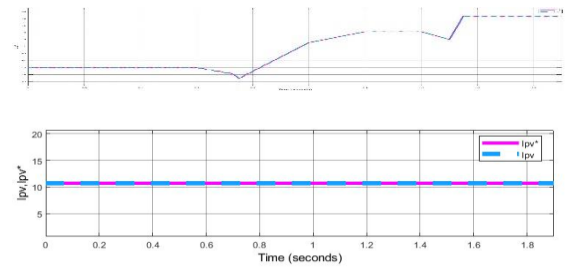Fig. 9. Dynamic performance at (a) ac side, (b) dc side, and (c) power flow when the system operates in Modes 3 and 4.
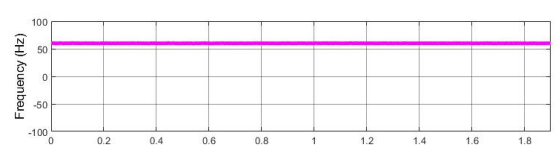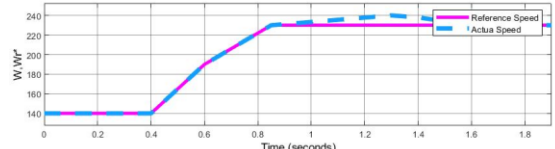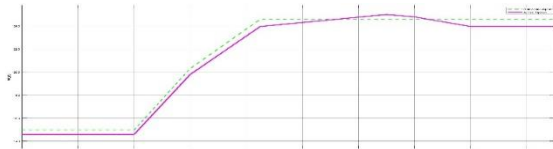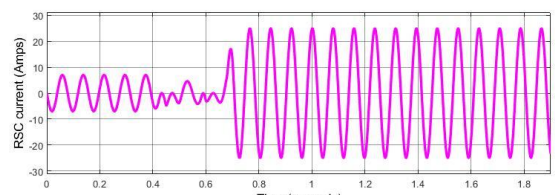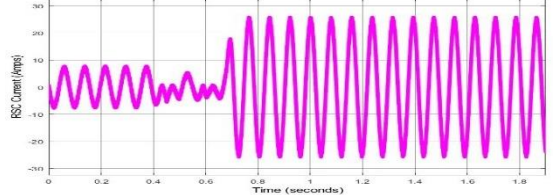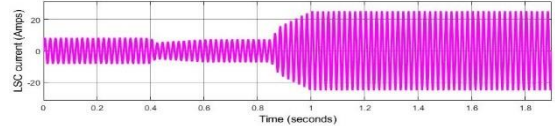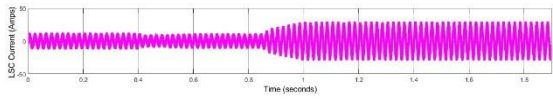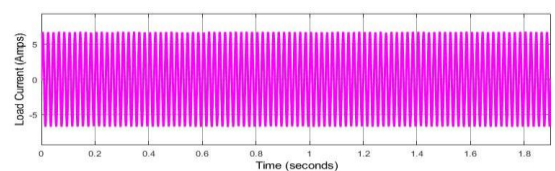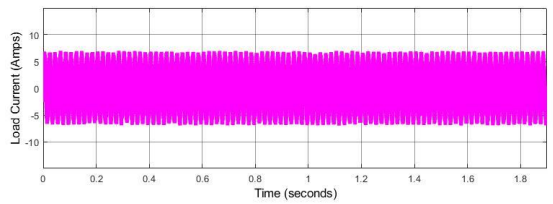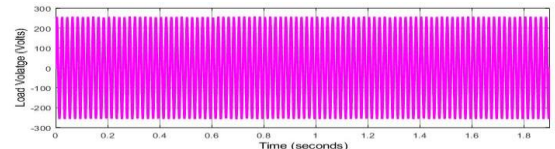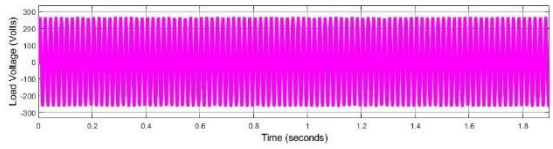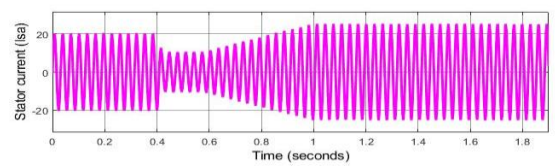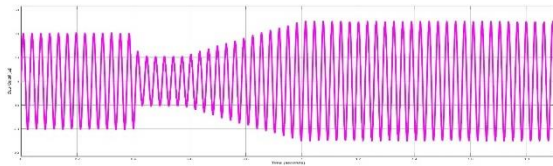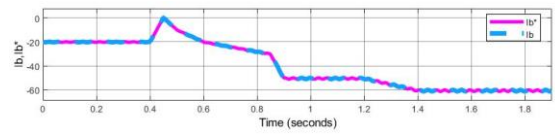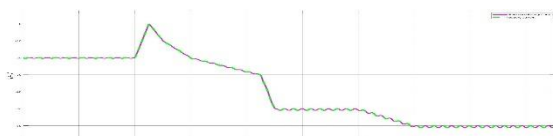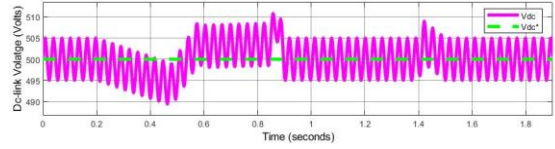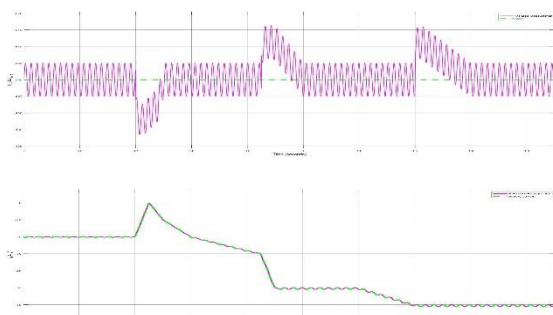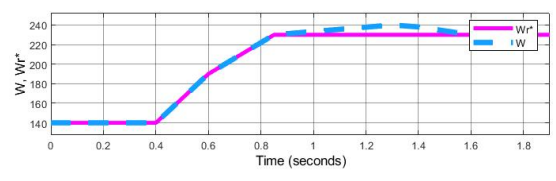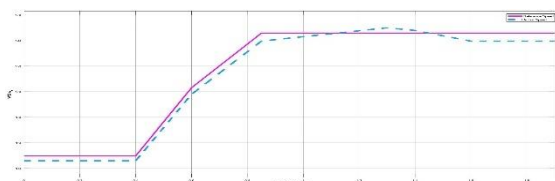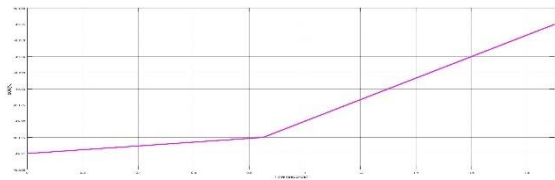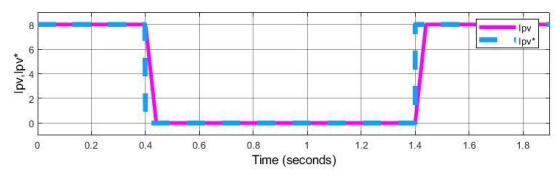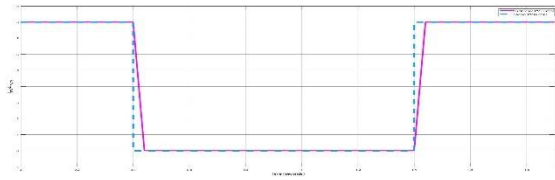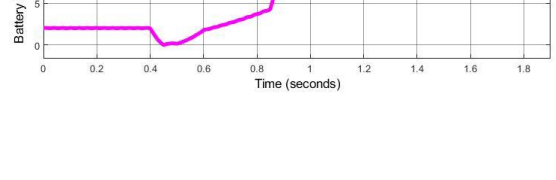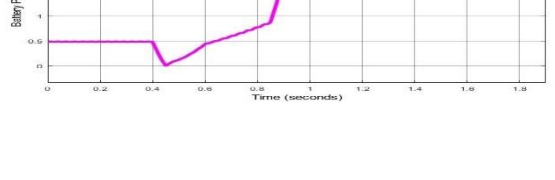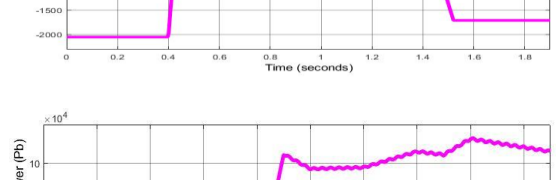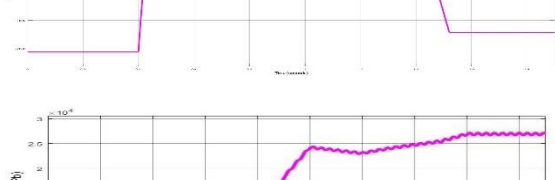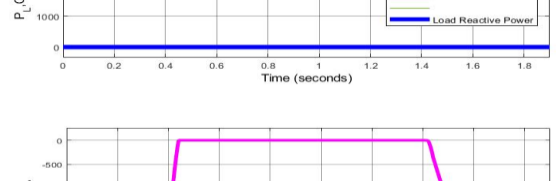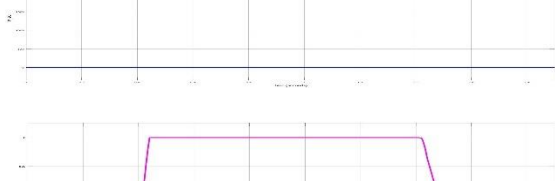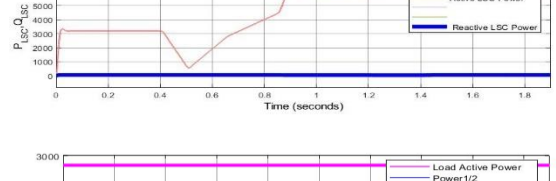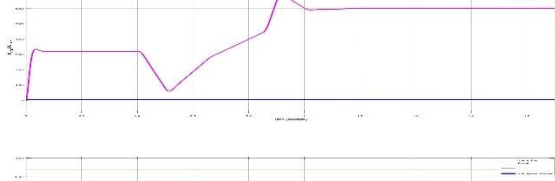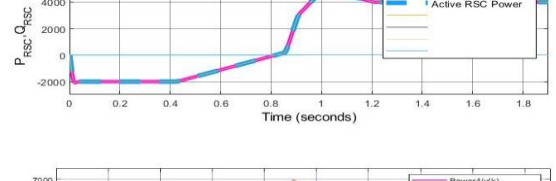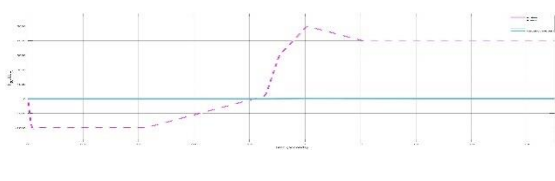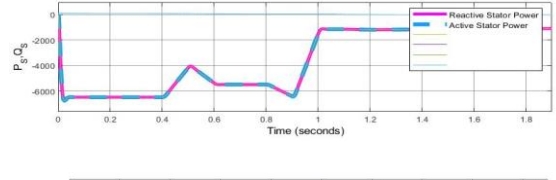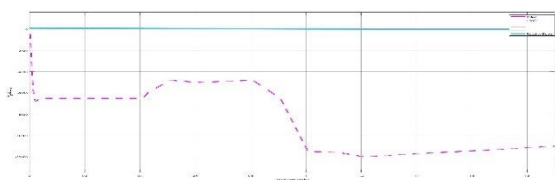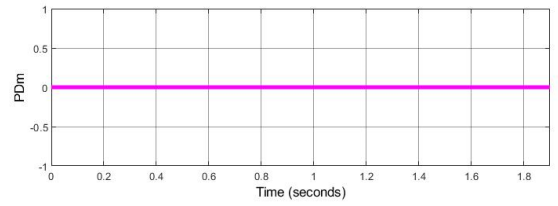
(c)

(a)

(a)

(b)

(b)

(c)

Fig. 10. Dynamic performance at (a) ac side, (b) dc side, and (c) power flow when the OFF-grid system operates in modes 5, 6, and 7.
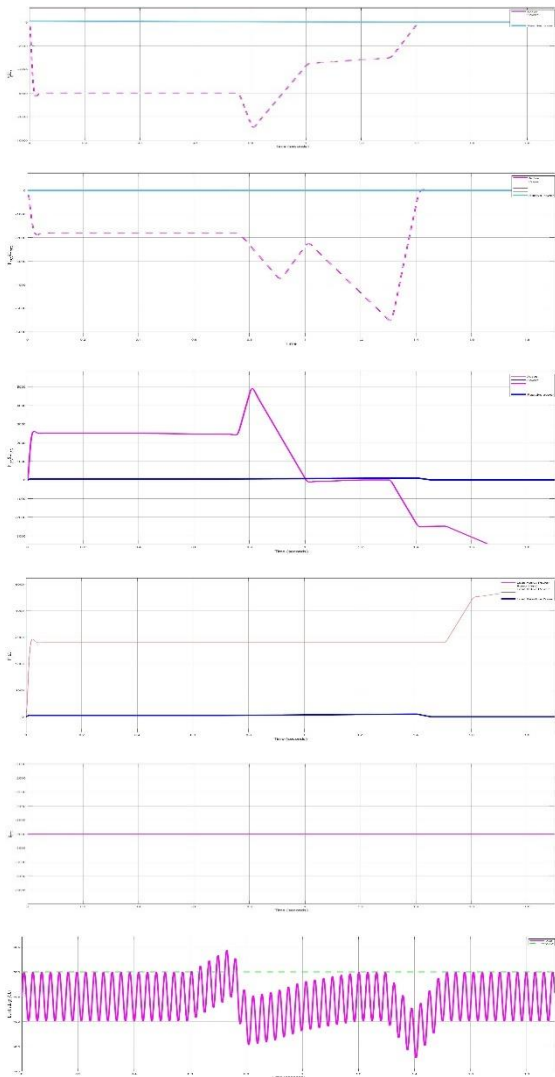

(c)

Fig. 10. Dynamic performance at (a) ac side, (b) dc side, and (c) power flow when the OFF-grid system operates in modes 5, 6, and 7.
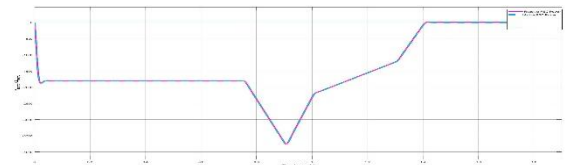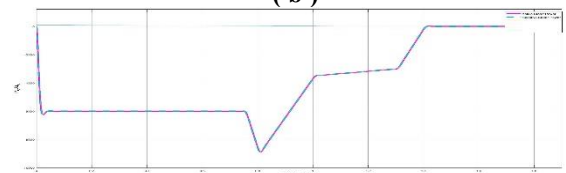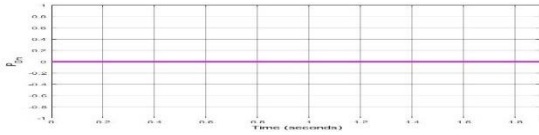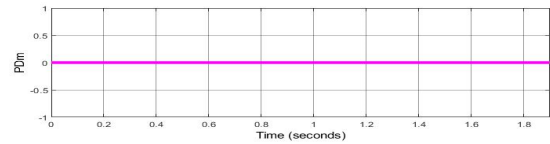

(a)
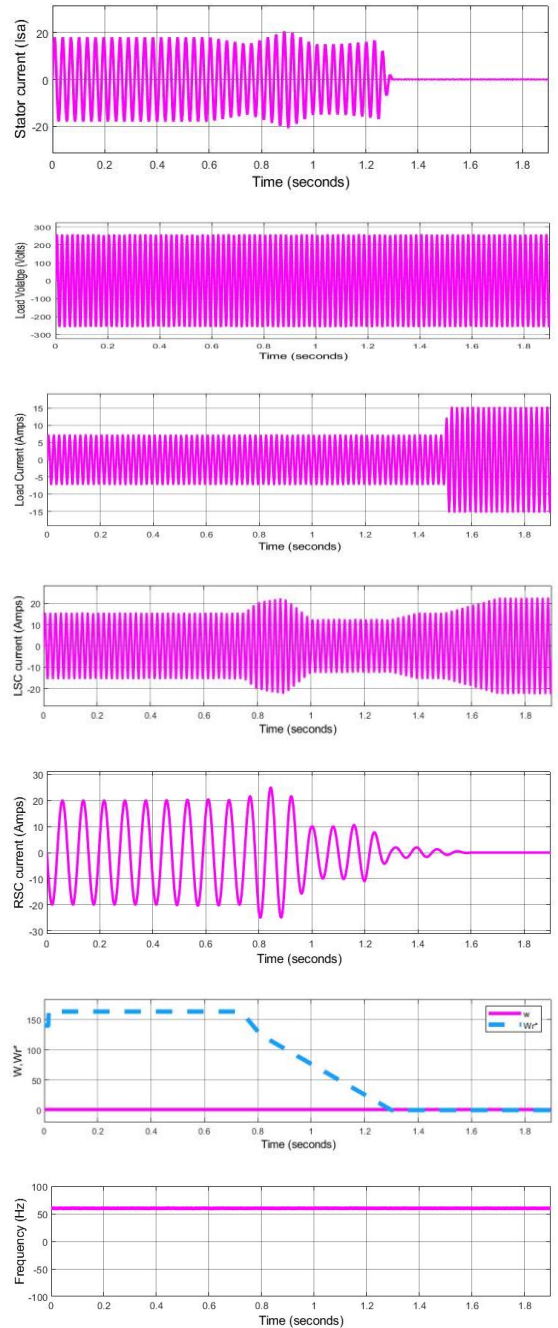
(a)
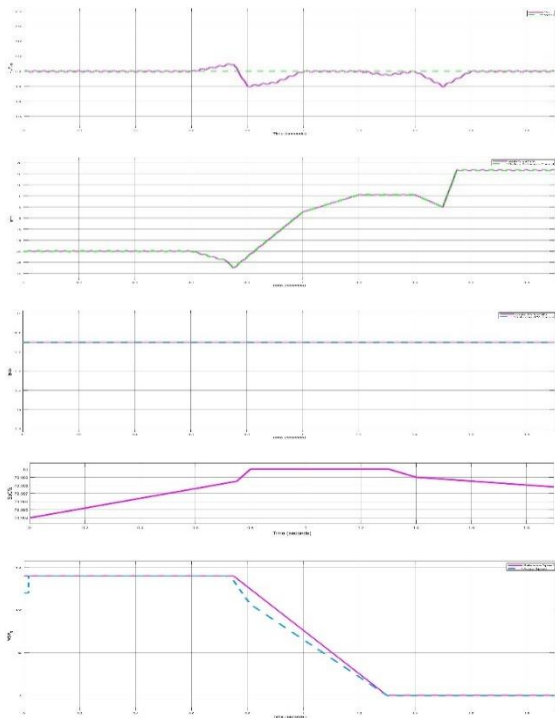
(b)
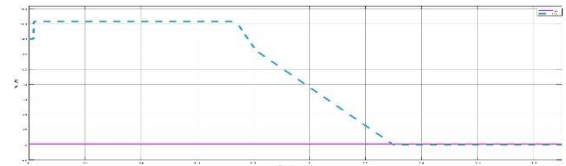
(b)
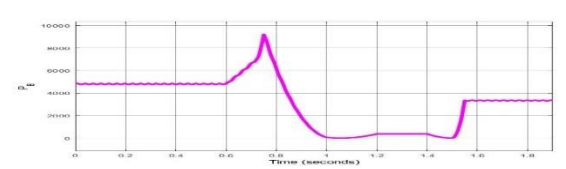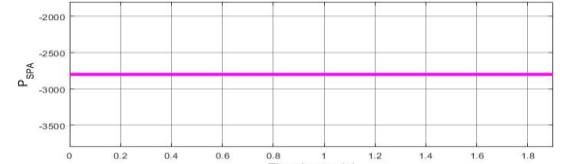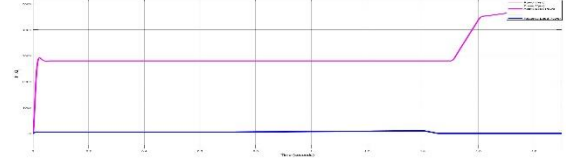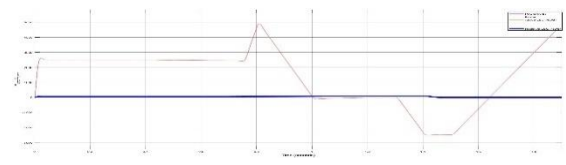
(c)

Fig. 11. Dynamic performance at (a) as side, (b) dc side, and (c) power flow when the system operates in Modes 8 and 9, and at sudden load increment.

Fig 8: Parameter	% of THD obtained by usingAWPI
Inverter Current	13.61% in Fig (1)
Load Current	13.61% in Fig (2)
Load Volage	13.83% in Fig (3)

Fig:-1

Fig:-2

Fig:-3

Fig-9: Parameter	% of THD obtained by usingAWPI
Inverter Current	10.12% in Fig (1)
Load Current	10.12%in Fig (2)
Load Voltage	10.12% in Fig (3)

(c)

Fig. 11. Dynamic performance at (a) as side, (b) dc side, and (c) power flow when the system operates in Modes 8 and 9, and at sudden load increment.

Fig-8: Parameter	% of THD obtained by using FLC
Inverter Current	3.64% in Fig (1)
Load Current	3.39% in Fig (2)
Load Voltage	3.39% in Fig (3)

Fig:-1

Fig:-2

Fig:-3

Fig-9: Parameter	% of THD obtained by using FLC
Inverter Current	3.40% in Fig (1)
Load Current	3.31% in Fig (2)
Load Voltage	3.40% in Fig (3)

Fig:-1
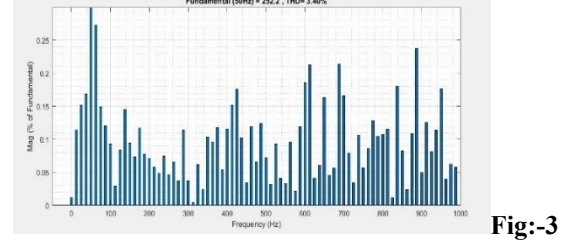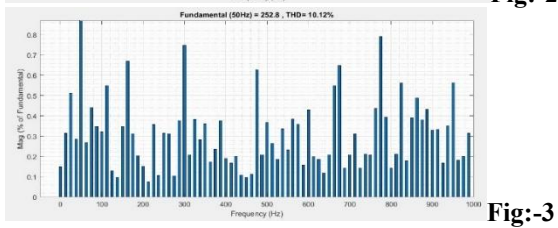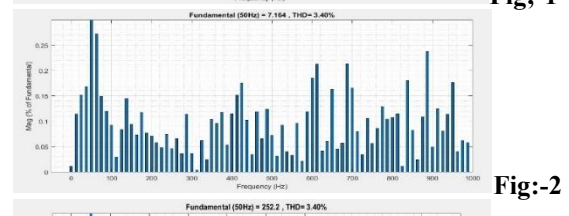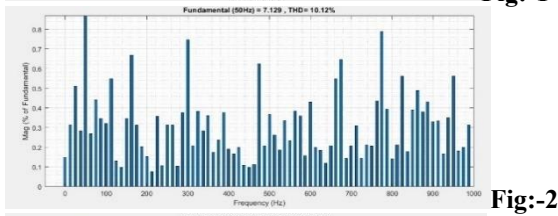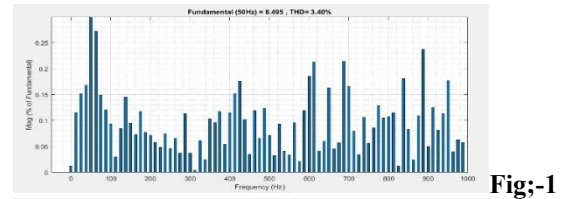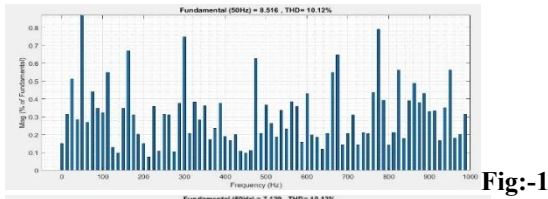
Fig:-2

Fig:-3

Fig-10: Parameter	% of THD obtained by using AWPI
Inverter Current	13.01% in Fig (1)
Load Current	79.79% in Fig (2)
Load Voltage	6.54% in Fig (3)

Fig;-1

Fig:-2

Fig:-3

Fig-10: Parameter	% of THD obtained by using FLC
Inverter Current	3.34% in Fig (1)
Load Current	3.77% in Fig (2)
Load Voltage	3.25% in Fig (3)

Fig:-1

Fig:-2
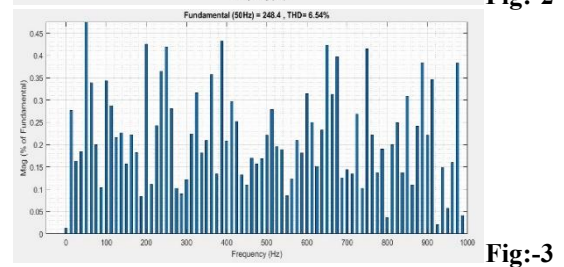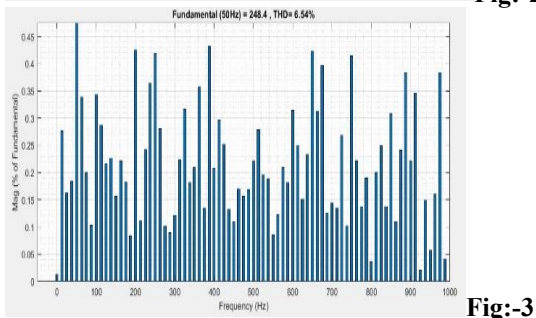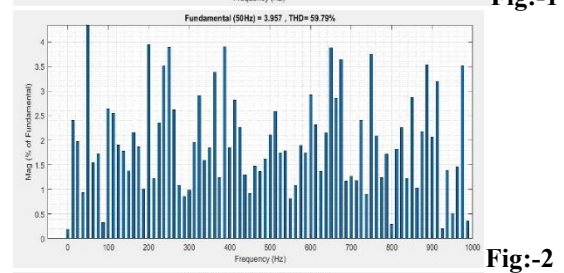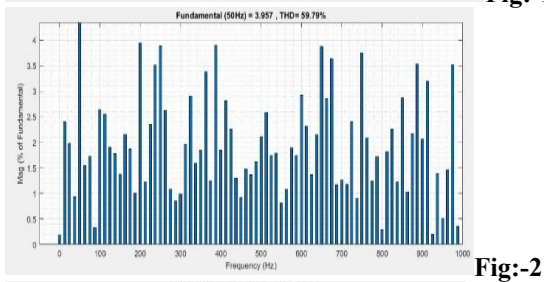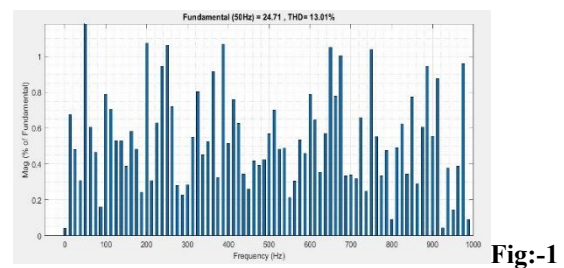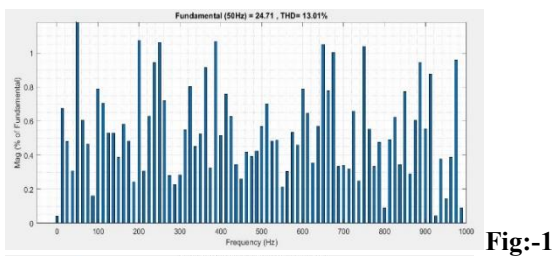
Fig:-3

Fig:-1

Fig:-2

Fig:-3

Fig-11: Parameter	% of THD obtained by using AWPI
Inverter Current	95.42% in Fig (1)
Load Current	82.13% in Fig (2)
Load Voltage	10.12% in Fig (3)

Fig-11: Parameter	% of THD obtained by using FLC
Inverter Current	3.46% in Fig (1)
Load Current	2.99% in Fig (2)
Load Voltage	3.39% in Fig (3)
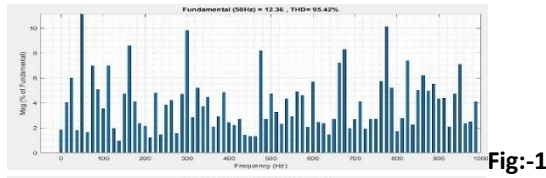
Fig:-1

Fig:-2

Fig:-3

Load Current

IN DIAGRAM PARAMETERS:-

Fig:-1

Fig;-2

Fig;-3

A Simulink dynamic model is created using the MATLAB Sim-Power system in order to analyze the performance of the hybrid DG-SPA OFF-grid system and its control techniques. A small scale prototype is constructed in the lab, as seen in Fig. 7. Every hybrid off-grid system operating mode listed in Table I is put to the test under various load variations and solar radiation conditions. Power flow as well as ac and dc side performances are shown for each test. The performance of the phase "a" stator current (i_{sa}), phase load voltage (V_L), phase "a" LSC current (i_{LSCa}), phase "a" RSC current (i_{RSCa}), rotor speed (w_r) and its reference (w_r^*), and system frequency (fs) are shown in Figs. 8–11(a).

Using the MATLAB Sim-Power system, a Simulink dynamic model is built to examine the hybrid DG-SPA OFF-grid system's performance and control strategies. As shown in Fig., a small-scale prototype is built in the laboratory. 7. We test all of the hybrid off-grid system operating modes described in Table I under a range of load and solar radiation fluctuations. For every test, power flow and both the ac and dc side performances are displayed. Figures display the performance of the following: rotor speed (w_r) and its reference (w_r^*), system frequency (fs), phase "a" stator current (isa), phase load voltage (V_L), phase "a" LSC current (i_{LSCa}), phase "a" RSC current (i_{RSCa}), and phase lock voltage (V_L).
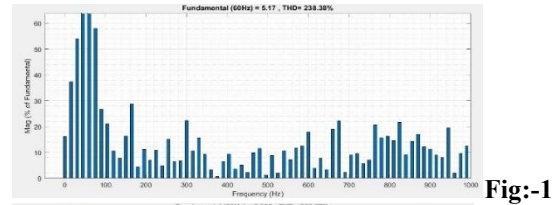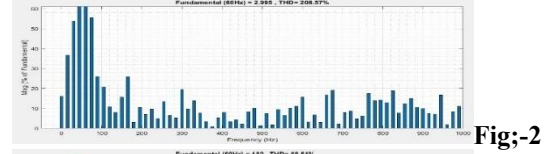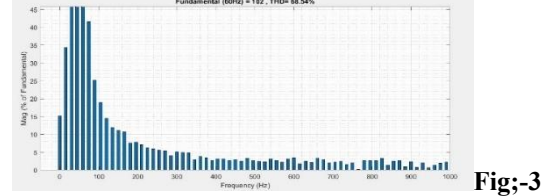
VII.CONCLUTION:-

The outcomes of the simulation are displayed in the technique above. The system's performance is very poor and the Antiwindup PI controller indicates the percentage of THD. The suggested Fuzzy controller will address these issues.

FUTURE SCOPE:

In the future, it may be possible to replace the fuzzy logic controller with an ANN or an ANFIC controller to achieve better controlled system performance.

REFERENCES:-

[1] M.Rezkallah,S.Sing,H.Ibrahim,Coordinated Control Strategy for Hybrid OFF-Grid System Based on Variable Speed Diesel Generator,IEEEDigital objective Identifier 10.1109/TIA.2022.3174825,4 July-August 2022.

[2] A. Accetta and M. Pucci, "Energy management system in DC micro-grids of smart ships: Main gen-set fuel consumption minimization and fault compensation," IEEE Trans. Ind. Appl., vol. 55, no. 3, pp. 3097–3113, May/Jun. 2019.

[3] Y. Bhandari, S. Chalise, J. Sternhagen, and R. Tonkoski, "Reducing fuel consumption in microgrids using PV, batteries, and generator cycling," in Proc . IEEE Int. Conf. Electro-Inf. Technol., 2013, pp. 1–4.

[4] R. É. PeÑa, R. Cárdenas, J. É. Proboste, J. Clare, and G. Asher, "Wind– diesel generation using

doubly-fed induction machines," IEEE Trans. Energy Convers., vol. 23, no. 1, pp. 202–214, Mar. 2008.

[5] S. K. Tiwari, B. Singh, and P. K. Goel, "Control of wind-diesel hybrid system with BESS for optimal operation," IEEE Trans. Ind.Appl., vol. 55, no. 2, pp. 1863–1872, Mar./Apr. 2019.

[6] M. Greig and J. Wang, "Fuel consumption minimization of variable-speed wound rotor diesel generators," in Proc. 43rd Annu. Conf. IEEE Ind. Electron. Soc., 2017, pp. 8572–8577.

[7] R. Miloud, A. Chandra, B. Singh, and S. Singh, "Microgrid: Configurations, control, and applications," IEEE Trans. Smart Grid, vol. 10, no. 2, pp. 1290–1302, Mar. 2019.

[8] T. Waris and C. V. Nayar, "Variable speed constant frequency diesel power conversion system using doubly-fed induction generator (DFIG)," in Proc. IEEE Power Electron. Specialists Conf., 2008, pp. 2728–2734.

[9] S. Puchalapalli, S. K. Tiwari, B. Singh, and P. K. Goel, "A microgrid based on wind-driven DFIG, DG, and solar PV array for optimal fuel consumption," IEEE Trans . Ind.Appl., vol. 56, no. 5, pp. 4689–4699, Sep./Oct. 2020.

[10] A. K. Birudula, R. Selvaraj, T. R. Chelliah, and U. S. Ramesh, "Improved fuel-use efficiency in diesel-electric tugboats with an asynchronous power generating unit," IEEE Trans. Transp. Electrific., vol. 5, no. 2, pp. 565–578, Jun. 2019.